Effective grid connection approach for an overshot waterwheel

Enfoque eficaz de conexión a la red de una rueda hidráulica de tipo overshot

Vicente Leite [ID] [1*]

[1]Research Centre in Digitalization and Intelligent Robotics (CeDRI), Instituto Politécnico de Bragança. Campus Santa Apolónia.5300-253. Bragança, Portugal.

ABSTRACT: Interest in very small-scale hydropower generation has increased over the past few years. These pico-hydro systems range from a few watts to several kW. The exploitation of low head sites does not require expensive civil works and is environmentally sustainable. Pico-hydro systems are attractive not only for remote areas where the grid is not available, but also for grid connection. This is especially relevant in existing infrastructures, used for other activities but which can also be used for energy generation. Waterwheels are emerging with enormous potential in this context. Low speeds and variations in head and water flow are a constraint to their connection to the grid. This study shows that they can be effectively connected to the grid using competitive and widely available technology for other renewable sources, such as photovoltaics. This paper presents an innovative approach for an effective grid connection of a pico-hydro system based on an overshot waterwheel. For this purpose, a permanent magnet synchronous generator and a photovoltaic inverter are used. The compatibility between them is analysed in detail and the analysis is valid for other hydro turbines. The 2 m diameter waterwheel has been installed on an existing infrastructure of an aquaculture centre. With a flow rate of about 13 l/s, it injects an average power of 126 W into a microgrid with a global efficiency of 50%.

RESUMEN: El interés por la generación hidroeléctrica a muy pequeña escala ha aumentado en los últimos años. Estos sistemas pico-hidráulicos van de unos pocos vatios hasta varios kW. La explotación de emplazamientos de baja altura no requiere costosas obras civiles, son ambientalmente sostenibles. Son atractivos no sólo para las zonas remotas donde no hay red, sino también para la conexión a la red. Esto es especialmente relevante en infraestructuras existentes, utilizadas para otras actividades, pero que también pueden utilizarse para la generación de energía. Las ruedas hidráulicas están surgiendo con un enorme potencial en este contexto. Las bajas velocidades y las variaciones en la altura y el caudal son una limitación para su conexión a la red. Este estudio demuestra que pueden conectarse eficazmente utilizando tecnología competitiva y ampliamente disponible para otras renovables, como la fotovoltaica. Este trabajo presenta un enfoque innovador para la conexión eficaz a la red de una rueda hidráulica *overshot*, utilizando un generador síncrono de imanes permanentes y un inversor fotovoltaico. La compatibilidad entre ambos se analiza en detalle y el análisis es válido para otras turbinas hidráulicas. Una rueda hidráulica de 2 m de diámetro se ha instalado en la infraestructura existente de un centro de acuicultura. Con un caudal de unos 13 l/s, ésta inyecta una potencia media de 126 W en una microrred con un rendimiento global del 50%.

1. Introduction

The world is facing the great challenge of our time: to reach net zero by 2050 and limit the rise of global

* Corresponding author: Vicente Leite
E-mail: avtl@ipb.pt

temperature to 1.5 °C. This requires, without further ado, a total transformation of energy systems. This definitely requires a total transformation of energy systems [1]. Indeed, energy is a critical economic and environmental development challenge that the world continues to face today [2].

Hydropower is a flexible, low‑emissions source of generation [1] and gives a significant contribution to the world energy demand with $4,370\ TWh$ electricity generated in 2020 [3]. Historically, it is associated with centralised generation based on big power plants [4, 5] with significant advantages, but also with no less significant disadvantages [6, 7]. Nowadays, energy generation is increasingly distributed [8] with great advantages, mainly when associated with microgrids [9–12].

Small-scale hydropower generation can be a fundamental foundation for sustainable development, public service delivery, as well as poverty alleviation. Despite the appeal and benefits of small-scale plants, 66% of their potential around the world remains untapped [3].

In the new paradigm of distributed generation and self-consumption, the integration of small and very-small hydro systems in the local context, through the optimized use of water resources, can positively impact on the local ecosystem [4, 13, 14]. These small systems, up to $5\ kW$ [6, 7, 15] or $10\ kW$ [4], are mentioned in the literature as pico-hydro systems. When integrated into existing infrastructures, their impact is twofold: renewable electricity generation and the spread of small-scale hydro systems.

In such applications, where electricity generation is not the main priority, those systems are designated as multipurpose schemes [13]. Thus, while the existing infrastructures continue to guarantee their primary function, they also generate energy at the same time.

Water supply systems, irrigation channels and wastewater treatment systems are just a few examples [4, 16, 17]. Under this purpose, this paper presents a pico-hydro system suitably integrated into existing infrastructure, which consists of using the water discharge for a tank at the Centro Aquícola de Castrelos (Castrelos' Aquaculture Centre), in Bragança, Portugal [18]. This work was carried out under the project BIOURB-NATUR - Bio constructive diversity, bioclimatic building, sustainable rehabilitation and application in natural parks, funded by European Commission - POCTEP.

During the last decades, small-scale water turbines have been used in off-grid pico-hydro systems in rural areas [14, 19] and some works present new developments for improved quality [20]. Recently, the development of these systems has gained new impetus through its use in new applications, such as: in hybrid systems with pumped-hydro energy storage [21], in microgrids for energy storage [22], or as a cost-effective and well-established way to generate electricity [9].

In fact, there is a wide use of pico-hydro systems, especially in off-grid systems, which are very popular in developing countries [4, 14, 23, 24]. However, despite the trigger of emerging applications, there are still knowledge gaps regarding the most effective approach for connecting them to the grid, which is one of the goals of the study presented in this work.

Recently, studies have been published based on two distinct approaches. The first consists of the development of specific control for the power electronics responsible for the generator operating point and grid interface [8, 10]. The second uses a more effective solution. This latter approach is based on the "plug and play" principle, with the integration of technology widely available on the market and at very competitive prices [25, 26].

This paper is intended as a relevant contribution to this second strategy. It is based on the proper integration of a permanent magnet synchronous generator (PMSG), widely used in small wind turbines [11, 27], and photovoltaic (PV) string inverters. In general, an over-voltage protection circuit is additionally required [28].

Water turbines used to generate electricity are a mature and widely spread technology, even for small hydropower plants [10, 23, 24]. In ancient times, more than 2000 years ago, waterwheels were an important discovery as hydraulic machines used to convert water energy into mechanical energy. They were extensively used for many centuries, in many applications, until they were replaced by the electric motor in the middle of the last century [29, 30]. Water turbines were considered a relic from the beginning of the industrial revolution [29].

During the last decades, due to new societal challenges related to environmental sustainability, the need to explore low head hydroelectric power sources to generate electricity became greater than ever [29].

Nowadays, waterwheels have become attractive again as water turbines for power generation. This happens not only where large distances usually require decentralized electricity production, and off-grid power plants, but also as a grid-connected system [10, 22, 25].

Waterwheels are environmentally friendly and can

help preserve cultural heritage [30], such as in the Silk House museum, where a waterwheel was installed in the place there was a former mill [31]. Moreover, they can contribute to the promotion of eco-tourism and social activities [30, 31], as in the present case of the BIOURB-NATUR project [18].

Most of the knowledge about waterwheels is very old, and there is a lack of information and uncertainty [32]. Therefore, several recent studies have been carried out to evaluate their performance and efficiency improvements [30, 32, 33], even for power ranges of just a few hundred watts [16].

Despite this recent interest in small-scale turbines, including waterwheels, there is still another challenge: how to connect to the grid in a cost-effective, robust and flexible way. This paper is an extended version of the work presented in [18] and is intended as an important contribution to this challenge. It proposes an effective (robust, flexible, efficient, economical and practical) grid connection approach, applied to an overshot waterwheel, which is based on inverters and generators widely available on the market.

The paper is organized as follows: after this introduction, the design of a waterwheel using a freely available tool [34, 35] is presented in section 2; the content of section 3 is intended as a relevant contribution to the state-of-the-art and presents the detailed design of an effective grid connection approach based on widely available components; section 4 presents the implementation details and experimental results; and section 5 presents the results and their analysis. Finally, the conclusions are presented in section 6.

2. Overshot waterwheel

Among all kinds of waterwheels, the overshot one presents the highest efficiency (up to 85-90%) over a wide range of water flows [33]. The overshot waterwheel is generally used for head differences of $2.5 - 10\ m$, and flow rates of $100 - 200\ l/s$ per metre width [29]. Unfortunately, the site conditions for implementing an overshot waterwheel at the Castrelos Aquaculture Centre do not completely satisfy the ideal site parameters. Indeed, the main channel that captures the water from the river has a flow of approximately $100\ l/s$ and the heads that can be exploited are low (less than $2.5\ m$).

After interviewing the people working at the Aquaculture Centre, and in order to suitably integrate the waterwheel into the existing infrastructures, it was designed to take advantage of the water falling into a tank.
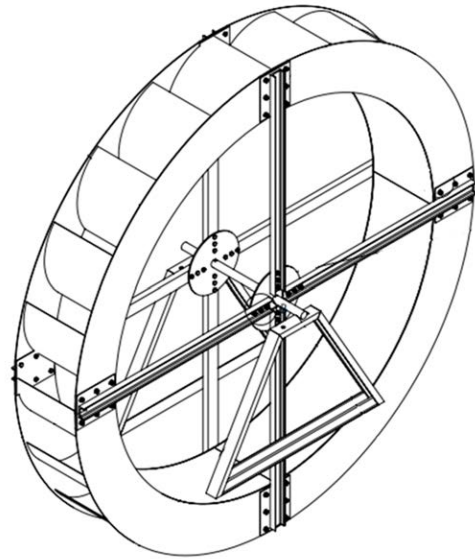

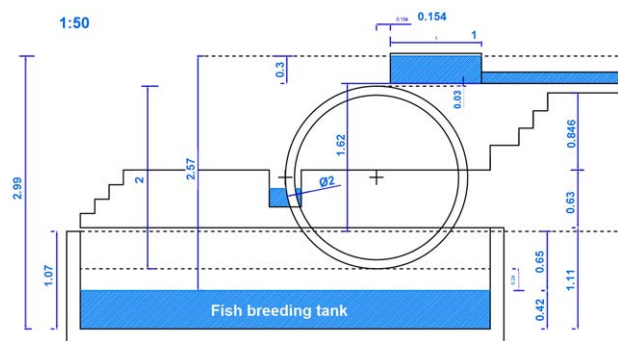**Figure 1** Draw of the designed overshot waterwheel by Luís Queijo

Figure 2 Implantation scheme in the fish breeding tank by Rui Oliveira

The highest head available was $2.5\ m$ and the flow rate was about $15\ l/s$ by the time of the data survey. Considering the efficiency of these waterwheels is approximately constant over a wide range of flow rates [29, 33], it was decided to design a wheel for $25\ l/s$ with a diameter of $2\ m$.

There are some recent works related to the design of waterwheels, namely the overshot type [32, 33, 35]. In this work, the platform available online [34] and the master's thesis [35] were used. Figure 1 shows a draw of the designed overshot waterwheel, and Figure 2 shows the implantation scheme in the fish breeding tank.

The waterwheel was built in stainless steel with 4 radial arms, $26\ cm$ width and a total of 20 buckets $26\ cm$ length, $20\ cm$ depth and $31.4\ cm$ width and spacing. The estimated rotational speed, at maximum power, is $6.8\ rpm$.

The estimated hydraulic power depends on the design water flow ($25\,l/s$) and the head available ($2\,m$) on the site. The generated mechanical power P (W) at the turbine shaft is estimated by Equation 1, as follows [36]:

$$P = \eta \times g \times \rho \times Q \times H \qquad (1)$$

where η is the turbine hydraulic efficiency, g is the acceleration due to gravity ($\simeq 9.8\,m/s^2$), ρ is the water density (= 1000 kg/m^3), Q is the water flow in the turbine (m^3/s), and H is the gross head (m).

Considering $g \simeq 10\,m/s^2$ and the water flow expressed in l/s, the mechanical power equation can be simplified by Equation 2, as follows:

$$P[W] \simeq 10 \times \eta \times Q[l/s] \times H[m] \qquad (2)$$

Assuming an overall efficiency (including waterwheel, gearbox, generator, cable, rectifier, and inverter) of 50%, the power injected into the grid will be $5 \times 25\,l/s \times 2\,m = 250\,W$.

3. Grid connection approach

Nowadays, the grid connection of small wind turbines and PV modules is a mature technology and spread worldwide [11, 37]. Therefore, PMSGs and PV inverters are widely available and at competitive prices. On the contrary, grid-connected pico-hydro systems are not widespread enough, as the level of standardization is low. In effect, for these systems, each solution is designed for the specific site requirements [14].

Anyway, PMSGs-based small-scale hydro turbines are emerging as grid-connected energy sources. The grid connection approach is described in the next sections and applied to the overshot waterwheel.

3.1 Methodology

The methodology used in this work to connect the waterwheel to the utility grid is shown in Figure 3. It consists of a suitable integration of a PMSG and a PV inverter. This approach has been investigated over the last few years [25, 26], including very small-scale hydro systems [25, 26, 28]. It is a viable alternative to the conventional way of connecting hydro generators to the grid [8, 36]. In fact, with this approach, the PMSG does not need to operate at a constant speed, close to the rated speed, and its operating point can vary within a wide operating range. In this way, the use of complex mechanical devices to control the generator speed is avoided.
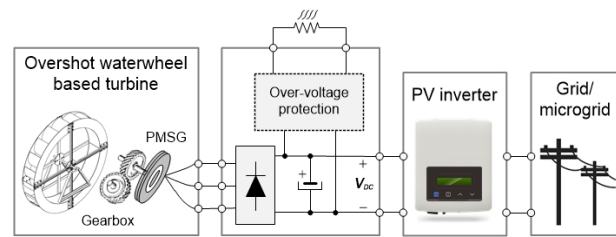

Figure 3 General grid connection scheme

The first stage of power conversion in Figure 3 is from hydraulic (Equation 1) to mechanical power, given by $\omega \times T$, where T is the torque (Nm) and ω is the waterwheel rotational speed (rad/s). Unfortunately, this speed is very low ($\leq 20rpm$) and operating speeds less than $10\,rpm$ are expected [32, 36]. Because of this drawback, a second mechanical power conversion stage is necessary, from low speed to higher speed (and lower torque). This is achieved through a high ratio gearbox, as illustrated in Figure 3. Even so, it may be necessary to use a low-speed PMSG, commonly used in small wind turbines. Indeed, from the calculator [34], the rotation speed of the waterwheel ($6.8\,rpm$). This is very low, even for PMSGs used in low-speed wind turbines, where the speed is in the range of some hundreds of rpm. Because of this constraint, and to achieve a rotational speed of not less than $300\,rpm$, a gearbox available on the market, with a gear ratio of 1:45 was selected.

The generator performs the third conversion stage, converting the shaft's mechanical power ($\omega \times T$) into AC electrical power, characterized by a three-phase voltage system. Next, a full-bridge rectifier converts these voltages into a DC voltage and current. After this fourth stage, the power (W) is given by $P = V_d \times I_d$, being V_d and I_d the average values of voltage and current, respectively, at the output of the rectifier bridge.

Last but not least, a fifth conversion stage (DC to AC) is needed to perform the interface with the grid. For this purpose, there are three available approaches: developing specific power converters [8, 25]; using wind turbine inverters; or using PV inverters [26]. The first requires a lot of development time, and several legal requirements must be accomplished. Even so, as with the second option, using wind inverters, the solution requires knowledge of the turbine's power curve and the consequent parameterization of the inverter. The third approach is the most "plug and play" of all and is based on widely available PV string inverters [25] or microinverters [26]. Whichever the approach, an over-voltage protection circuit is most likely required [28], as illustrated in Figure 3.

Unfortunately, the third approach is not completely universal. The compatibility of the PV inverter with a pico-hydro turbine depends on the maximum power point tracking (MPPT) algorithm and mainly on the way it is initialized [38]. For the PV inverters to be compatible with a water turbine, it is still necessary to make compatible the operating point range of both: the generator (ω,T) and inverter (V_{dc},I_{dc}). Next section presents a more in-depth development of this compatibility.

3.2 Compatibility analysis

The set consisting of the PMSG and the full-bridge rectifier can be described as a single-stage conversion of the shaft mechanical power into the DC electrical power at the input of the inverter. From the perspective of this power conversion stage, it is important to analyse, in some detail, the relationship between the operating point at the input (on the generator shaft) and at the output of the full-bridge rectifier.

Analysis of conversion from mechanical power to DC electrical power

Figure 4 presents the three-phase steady-state equivalent circuit of a non-salient PMSG and diode rectifier followed by a DC source modeling the input stage of the PV inverter. Indeed, in most cases, for the pico-hydro power range, the input stage of the PV inverter consists of a DC/DC converter or a high-frequency DC/AC converter [39]. In addition to operating with an output voltage much higher than the input, this input stage makes the modules operate at their maximum power point (MPP).

From the point of view of its input, the PV inverter behaves like a dynamic resistor, adjusting the voltage (through the MPPT algorithm) in order to maximize the power and, therefore, maximize the current for the MPP voltage. In this way, it is possible to model the PV inverter (viewed from the input), as a current source [27] as shown in Figure 4, where X is the reactance due to stator winding (X_s) and line (X_L), R corresponds to the stator (R_s) and line (R_L) resistances, and V_s and I_s are, respectively, the

Figure 4 Steady-state equivalent circuit of PMSG, transmission line, diode rectifier and PV inverter

stator phase voltage and current of the non-salient PMSG. The induced electromotive voltage in the stator winding (E) is directly proportional to the electrical angular speed (rad/s). V_d and I_b are, respectively, the output DC voltage and current of the rectifier.

The average output voltage of the three-phase full-bridge diode rectifier is given by Equation 3, where $V_{d,o.c.}$ is the DC open-circuit voltage, and $\triangle V_d$ corresponds to voltage drop due to generator and line inductances ($L_s + L_L$), resistances ($R_s + R_L$) and across the diodes.

$$V_d = V_{d,o.c.} - \triangle V_d \qquad (3)$$

The first term of Equation 3 is given by $V_{d,o.c.} = \frac{3}{\pi} \times \sqrt{2} V_{LL}$ [40], being V_{LL} the generator's open circuit line-to-line voltage. Furthermore, $V_{LL} = \sqrt{3}E$ and the amplitude of the induced electromotive voltage, E_m, is given by $\sqrt{2}E$. On the other hand, $E_m = k_E\omega$, being k_E the generators' speed constant. Therefore, the first term of Equation 3 can be replaced by Equation 4:

$$V_{d,o.c.} = \frac{3\sqrt{3}}{\pi} k_E\omega \qquad (4)$$

It is clear that $V_{d,o.c.}$ is directly proportional to the electrical angular speed, as shown by Equation 4.

Due to the presence of the reactance $X = X_s + X_L$, the current commutation from one diode to the other in the rectifier bridge, does not occur instantaneously. It takes a time interval and consequently, during this interval, two upper diodes (and one lower diode), or two lower diodes (and one upper diode) will conduct simultaneously. Thus, during this commutation interval, one of the line-to-line voltages is equal to zero, while the other two are equal to V_d or $-V_d$. Therefore, the second term in Equation 3, $\triangle V_d$, is equal to $\frac{3}{\pi}\omega LI_d$, provided that the voltage drop in the rectifier's diodes and across the resistances ($R_s + R_L$) are neglected [27, 40]. Thus, Equation 3 can be rewritten as shown in Equation 5:

$$V_d \simeq \frac{3\sqrt{3}}{\pi} k_E\omega - \frac{3}{\pi}\omega LI_d \qquad (5)$$

From Equation 5, it is clear that, for each operating point, the DC input voltage at the PV inverter is proportional to the generator's rotational speed, as shown in Equation 6:

$$V_d \simeq \left(\frac{3\sqrt{3}}{\pi} k_E - \frac{3}{\pi} LI_d \right) \omega = K\omega \qquad (6)$$

Another important relationship for the analysis of the compatibility between the operating point of the generator and the PV inverter is the relationship between the torque
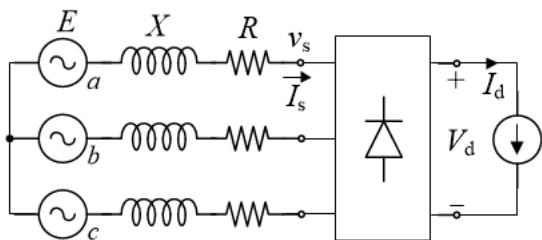
and the DC current at the output of the rectifier.

It is well known, from the control perspective, that torque is proportional to the stator current amplitude because the current space-phasor leads the rotor flux space-phasor by 90º, in order to maximize the torque [40].

Another perspective results from the dynamic modeling in the dq synchronous reference frame. In this case, the torque is proportional to the stator current quadrature component [27], which is supposed to be a DC current. Unfortunately, this relationship is not so straightforward [41]. Indeed, the nonlinearity caused by the full-bridge rectifier makes significant harmonics appear in the stator current, as well as in its quadrature component in the synchronous reference frame.

The relationship between the amplitude of the fundamental component of the generator current and the DC current at the output of the rectifier is $I_s = \frac{2\sqrt{3}}{\pi} I_d$, but the generator current also has harmonics of order $6k\pm1$, $k = 1, 2, 3, \cdots$ [42].
The relationship between I_s and I_d has already been deepened in some works for the case where the generator is connected to a three-phase full bridge rectifier. For instance, [43] addresses the analysis with constant-voltage loads and [27] considers a constant DC load current. In the latter case, the load current is controlled by a boost converter to control the operating point of a wind turbine.

In the context of grid-connected pico-hydro systems, as illustrated in Figure 3, the commercial PV inverter does not expect to have a hydro-power source instead of a PV one, at the input side. Thus, what is known is that, from the input side, it behaves like a dynamic resistance, adjusted according to its MPPT algorithm, so that the operating point corresponds to the maximum power point. It is very likely that the frequency of this tuning is less than a few Hz [38]. On the other hand, the input current controller bandwidth is certainly much higher. Furthermore, the most common situation of PV inverters is to have a high inductance at the input power stage, e.g., the inductance of a boost converter [27]. For these reasons, the PV inverter was modeled as a current source, as shown in Figure 4 and hence the result of Equation 5. Under these conditions, the authors in [27] deduce, in some detail, the relationship between the torque and the current I_d, as described in Equation 7:

$$T \simeq \frac{3\sqrt{3}}{\pi} N_p \phi_{fd} I_d = K_1 I_d \qquad (7)$$

where N_p is the number of pole pares and ϕ_{fd} is the amplitude of the flux linkage in the stator winding due to permanent magnets in the rotor.

Equation 7 shows that the electromagnetic torque is proportional to the DC output current of the rectifier. The same conclusion can be easily obtained by equating the generator's shaft power to the rectifier's DC output power, taking into account the efficiency (η_{g+r}) of both (generator+rectifier), i.e., $\eta_{g+r} \times \omega \times T = V_d \times I_d$, and approximating V_d by Equation 4. Then, after some elementary manipulations, Equation 8 is obtained.

$$T \simeq \frac{3\sqrt{3}}{\pi \times \eta_{g+r}} K_E I_d = K_2 I_d \qquad (8)$$

Knowing that $E = k\omega\phi_{fd} = K_E\omega$ it follows that both Equations 7 and 8 are basically the same.

The next section presents the analysis of the compatibility of the DC power, at the output of the bridge rectifier, with the PV inverter.

Analysis of the compatibility of the DC power with the PV inverter

This section focuses on the analysis of the compatibility between the DC output power of the generator and the PV inverter input, in the context of Figure 3. Considering Equations 6 and 8, it results that the PV inverter controls the operating point of the waterwheel (turbine), i.e., the rotational speed and torque. This is accomplished by controlling, respectively, the voltage V_d and current I_d at the output of the rectifier bridge. Furthermore, an additional goal was to find a "plug and play" approach to avoid the over-voltage protection circuit, as shown in Figure 5.

Generally speaking, the compatibility between the generator (and, therefore, the waterwheel) and the PV inverter consists of assuring that the operating points of both are inside a common area of their respective safe operating areas (SOAs). Figure 6 presents the SOAs of the Solax X1-0.7 PV inverter and 80-7s-2p PMSG, which were used in the implementation, as will be described in section 4.

The compatibility is ensured by sizing the operating point (I_{DC}, V_{DC}), in a common zone of the generator and inverter operating areas, as illustrated in Figure
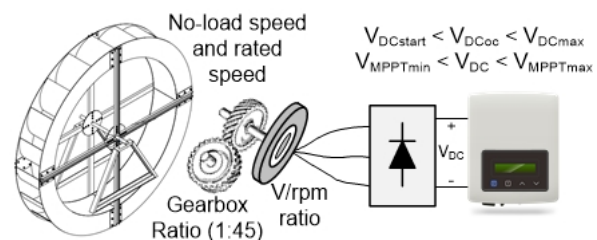

Figure 5 Grid connection scheme for the overshot waterwheel

6. According to Figures 5 and 6, in order to ensure this requirement, it is necessary:

1. To determine the waterwheel rotational speed (in normal and no-load operation);

2. To select the gearbox ratio and the generator V/rpm constant;

3. To check whether, for the minimum water flow, the open circuit (no-load) voltage is higher than the minimum voltage necessary for the inverter to start operating ($V_{DCoc} > V_{DCstart}$);

4. To check that, for the maximum water flow, the voltage does not exceed the inverter's maximum voltage ($V_{DCoc} < V_{DCmax}$);

5. And, finally, to confirm that the operating voltage, for the expected variations in head and water flow, is within the inverter's MPPT range ($V_{MPPmin} < V_{DC} < V_{MPPmax}$).

These requirements also apply to other turbines and PV inverters.

4. Implementation and experimental results

This section describes the on-site implementation of the constructed overshot waterwheel and the validation of the grid connection approach, as described in the previous section.

Figure 7 shows the overshot waterwheel installed in the fish tank. The flow rate was measured indirectly by averaging several counts of the time it took a colored spot to travel through the inlet pipe. The flow rate obtained was about $13\,l/s$.

Figure 7 Stainless steel overshot waterwheel installed in the fish tank
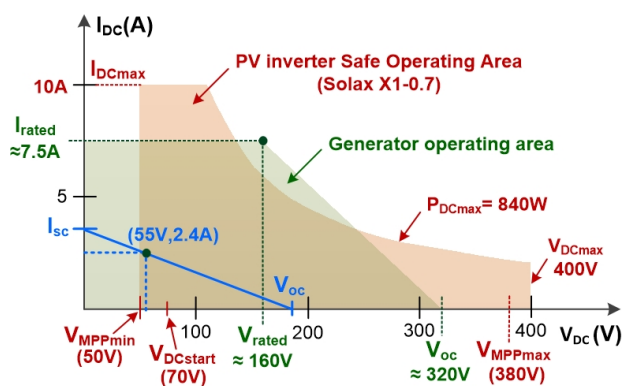
Figure 6 Overlap of the safe operating areas of Solax X1-0.7 PV inverter and 80-7s-2p generator

During the tests carried out over the first six months of 2021, at different times, the no-load rotational speed of the wheel varied between 22.5 and 25.5 rpm. The speed under load, around the maximum power, and for the flow available at each moment, varied between 7.8 and 12 rpm. For the initial design requirements, the expected operating speed was 6.8 rpm (with 25 l/s).

Taking into account the 1:45 speed ratio of the selected gearbox, the shaft speed of the generator is in the range $351 - 540\,rpm$. At no-load conditions, this speed reaches $1148\,rpm$. According to section 3.2, this speed must be higher enough to generate a DC voltage at the rectifier output, higher than the starting operating voltage of the PV inverter ($V_{DCoc} > V_{DCstart}$). On the other hand,

the rectifier's output voltage should be sufficiently lower than the maximum value of the DC input voltage of the PV inverter ($V_{DCoc} < V_{DCmax}$). Otherwise, the grid connection will not be completely "plug and play", being necessary to use an over-voltage protection circuit [28]. Furthermore, the DC operating voltage, around the MPP of the turbine, must be within the MPPT voltage range of the PV inverter ($V_{MPPmin} < V_{DC} < V_{MPPmax}$). Therefore, a suitable rated voltage of the generator, or speed constant V/rpm, must be selected for a given PV inverter or, for a given inverter, the rated speed of the generator must be conveniently selected, together with the gearbox ratio.

In practice, the solution design is an iterative process and considers the equipment available on the market and its cost. Fortunately, for the power in question, new inverters are being launched on the market with a wide MPPT range, where the lower limit is getting smaller. For instance, from the datasheets of the Solax X1-0.6 and Solis-mini-700-4G PV inverters, it can be seen that the lower limit of the MPPT range is, respectively, 45 and $50\ V$. On the other hand, the maximum voltage of input is high enough, respectively 450 and $600\ V$, to make the over-voltage protection circuit unnecessary.

To connect the waterwheel to the utility grid, the Solax X1-0.7-S-D(L) inverter was purchased with maximum DC input power $840\ W$, maximum DC input voltage $400\ V$, MPPT voltage range $55 - 380\ V_{DC}$ and start operating voltage $70\ V_{DC}$.

Additionally, tests were carried out with three different generators connected to the gearbox and waterwheel. The first was a low-speed axial flux permanent magnet generator, AFPMG260, designed for small wind turbines. The rated output power, speed, DC voltage and DC current are, respectively, $300\ W$, $300\ rpm$, $28\ V_{DC}$, $10.71\ A_{DC}$. The stator is star connected and the DC values refer to the output of the three-phase rectifier.

The second generator was a higher voltage PMSG, PGS 100R-WB 488, with the following rated characteristics: $800\ W$, $1500\ rpm$, $385\ V_{AC}$, $1.25\ A_{AC}$. This is a $100\ Hz$, 8 pole axial PMSG and these nameplate values are for star connection. In this work, the stator connections were reconfigured from star to delta to reduce the voltage.

The third generator is based on a three-phase BLDC (Brushless DC) electrical machine working as a permanent magnet alternator [44]. This is a lower-cost solution for small power applications. To operate as a generator, like the previous two, it is connected to a three-phase rectifier and the DC output voltage constant is $0.199\ V/rpm$ (under no-load). It is based on
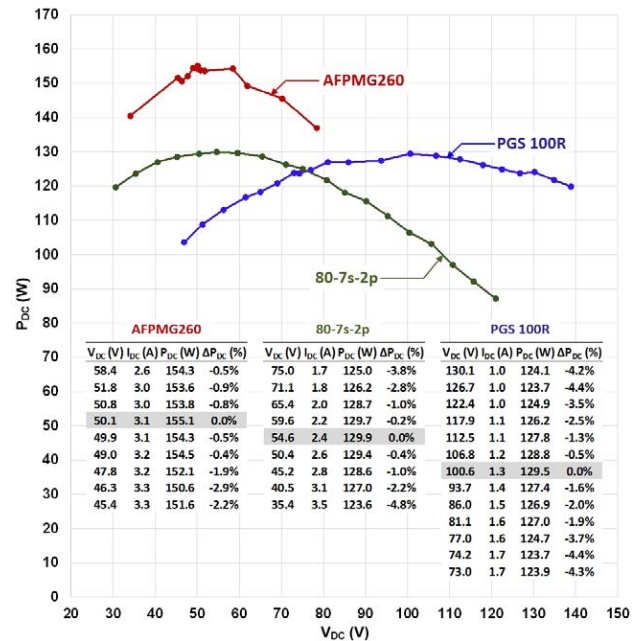

AFPMG260				80-7s-2p				PGS 100R			
V_{DC} (V)	I_{DC} (A)	P_{DC} (W)	ΔP_{DC} (%)	V_{DC} (V)	I_{DC} (A)	P_{DC} (W)	ΔP_{DC} (%)	V_{DC} (V)	I_{DC} (A)	P_{DC} (W)	ΔP_{DC} (%)
58.4	2.6	154.3	-0.5%	75.0	1.7	125.0	-3.8%	130.1	1.0	124.1	-4.2%
51.8	3.0	153.6	-0.9%	71.1	1.8	126.2	-2.8%	126.7	1.0	123.7	-4.4%
50.8	3.0	153.8	-0.8%	65.4	2.0	128.7	-1.0%	122.4	1.0	124.9	-3.5%
50.1	3.1	155.1	0.0%	59.6	2.2	129.7	-0.2%	117.9	1.1	126.2	-2.5%
49.9	3.1	154.3	-0.5%	54.6	2.4	129.9	0.0%	112.5	1.1	127.8	-1.3%
49.0	3.2	154.5	-0.4%	50.4	2.6	129.4	-0.4%	106.8	1.2	128.8	-0.5%
47.8	3.2	152.1	-1.9%	45.2	2.8	128.6	-1.0%	100.6	1.3	129.5	0.0%
46.3	3.3	150.6	-2.9%	40.5	3.1	127.0	-2.2%	93.7	1.4	127.4	-1.6%
45.4	3.3	151.6	-2.2%	35.4	3.5	123.6	-4.8%	86.0	1.5	126.9	-2.0%
								81.1	1.6	127.0	-1.9%
								77.0	1.6	124.7	-3.7%
								74.2	1.7	123.7	-4.4%
								73.0	1.7	123.9	-4.3%

Figure 8 $P - V$ curves of the waterwheel with 3 different generators

a delta-connected 80-7s-2p stator with 42 poles and a rotor type 2 ($0.75\ W/rpm$). According to [44], the rated output power, speed, DC voltage and DC current are, respectively, $1200\ W$, $1600\ rpm$, $180\ V$ and $6.7\ A$.

The tests with generators AFPMG260, PGS 100R and 80-7s-2p were performed on site, respectively, on 21 December 2020, 23 February 2021 and 9 June 2021.

To identify the point of maximum power, for the available flow rate, the curves P_{DC} versus V_{DC} were obtained, through the variation of load resistance. The results are presented in Figure 8. This figure also presents the values of DC voltage and DC current for a power variation of less than 5%, around the MPP. The values of the voltages and currents presented in Figure 8, and used to calculate the DC power, correspond to the average of 3 to 5 readings.

Figures 9 and 10 show the tracing of the DC power and current curves, respectively, as a function of DC voltage. The curves were obtained with the 80-7s-2p generator, for three different water flows. Figure 9 shows that the power curves have a well-defined MPP zone, and the voltage value corresponding to the MPP increases with the flow rate. It can be seen that the shape of the $P_{DC} - V_{DC}$ curves is similar to the corresponding curves of a PV string. Figure 10 shows that the $I_{DC} - V_{DC}$ curves have a very different shape to those obtained with a PV string.

Usually, $T - \omega$ curve is approximated by a straight line

[45, 46]. According to Equations 6 and 7 the relationship $I - V$ should also be linear. However, Figures 9 and 10 show that neither the $P - V$ curves are a perfect inverted parabola, nor the $I - V$ curves are linear.

The waterwheel was connected to the grid using the PV inverter Solax X1-0.7, either with generator 80-7s-2p or generator PGS 100R. Unfortunately, the inverter was not yet available when the AFPMG260 generator was attached to the waterwheel.

Figure 11 shows the first 4 minutes of the waterwheel connection to the grid. The maximum AC power obtained with the 80-7s-2p generator was $137\ W$ and $130\ W$ with generator PGS 100R. The average AC power, during the last minute, was $125.8\ W$ and $119.6\ W$, respectively.

The waterwheel speed under no-load was $25\ rpm$, and under load operation, it was $9\ rpm$ with generator 80-7s-2p and $11\ rpm$ with generator PGS 100R. Obviously, due to the gearbox, the shaft speed of the generator is 45 times higher.

Actually, using the approach described in this work, the waterwheel was connected to a smart microgrid, as illustrated in Figure 12. The microgrid is based on the SMA Flexible Storage System with battery backup function and increased self-consumption [47]. It uses 3 bidirectional inverters (Sunny Island 6.0H) [48], in a master-slave configuration, which are connected to a 48 V, 625 Ah battery bank. The microgrid also integrates a 10 kWp PV system using the multi-string inverter STP10000TL-20. The energy management and power control are performed by the battery inverters and by an energy manager (Sunny Home Manager) [49]. The microgrid was installed under the Project BIOURB-NATUR and the implementation details are out of the scope of this work.
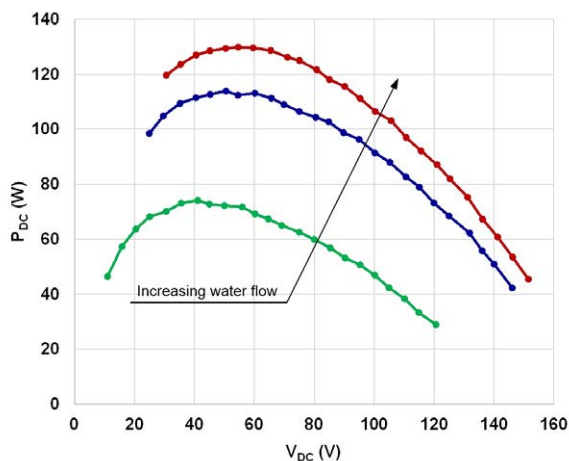
5. Analysis and discussion

Tests with the different generators were carried out at different times of the year and, most likely, with different flow rates. Without a water flow meter available on site, it is not possible to accurately relate the power to the water flow values, but this limitation does not compromise the objectives of the work. In fact, the most relevant data were accurately measured, namely DC power (by measuring DC current and DC voltage) and AC power, in steady-state and during grid connection. Thus, with the method used to measure the flow rate, it is not possible to accurately compare the DC power values obtained with the three generators shown in Figure 8.

As illustrated in Figure 5, by choosing a suitable gearbox ratio and a generator V/rpm constant, the operating DC voltage, at the output of the rectifier bridge, will be within the MPPT range of the PV inverter. Thus, the PV inverter will adjust its input voltage, through the MPPT algorithm, in order to extract the maximum power. On the other hand, if its maximum value, under no-load operation, is less than the maximum DC voltage at the inverter input, the over-voltage protection circuit can be avoided, as shown in Figure 5.

By analysing Figure 8, and considering a variation less than 5% around the MPP, it can be seen that the DC voltage range is $45.4 - 58.4\ V$, $73 - 130.1\ V$ and $35.4 - 75\ V$ for generators AFPMG260, PGS 100R and 80-7s-2p, respectively. Although the MPPT range on the nameplate of the PV inverter is $55 - 380\ V$, in practice, the lower limit is around $50\ V$. Thus, the inverter works close to the lower limit of its MPPT range with generators AFPMG260 and 80-7s-2p and inside the first quarter of the MPPT range with the generator PGS 100R.
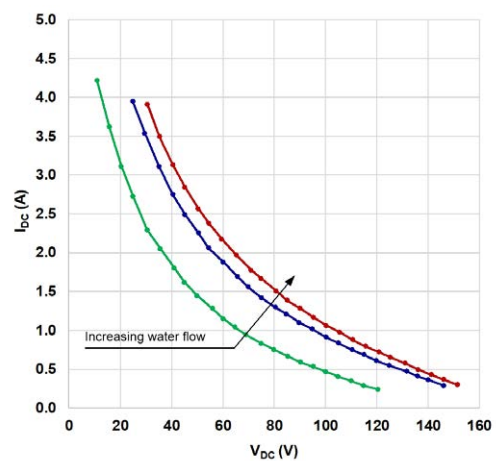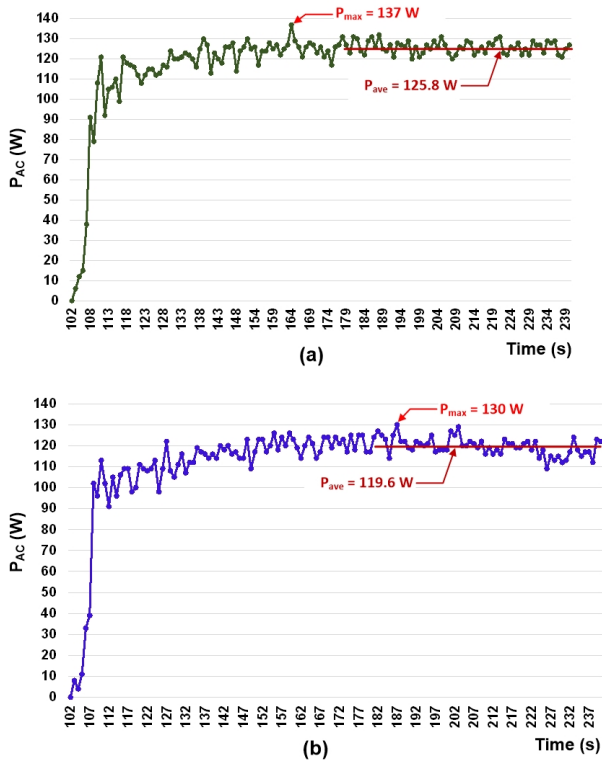

Figure 9 P_{DC}-V_{DC} characteristics for different water flows

Figure 10 I_{DC}-V_{DC} characteristics for different water flows

(a)

(b)

Figure 11 Grid connection of the overshot waterwheel using PV inverter Solax X1-0.7 and generators: (a) 80-7s-2p and (b) PGS 100

As illustrated in Figure 5, after the gearbox has been selected with a high transmission ratio (1:45 in this case), a generator with a suitable voltage constant (V/rpm) must be selected. In fact, there is a compromise: on the one hand, this constant must be large enough so that the voltage around the MPP is within the MPPT range of the inverter and, on the other hand, it must be small enough so that under no-load operation, the voltage does not exceed the upper limit of the inverter's input voltage ($400\,V$ in this case). Otherwise, an over-voltage protection circuit would be required.

It must be taken into account that the voltage constant (V/rpm) of the generator on load can be significantly lower than its value under no-load operation. For example, for the 80-7s-2p generator, the value at maximum output power was expected to be in the range $55\% - 60\%$ of the value under no-load [44]. However, according to the tests carried out, it was about 31%.

Figure 11 shows the evolution of the AC power injected into the grid (at the inverter output) during a start-up with generators 80-7s-2p and PGS 100R. The Solax X1-0.7 inverter took about 100 seconds to start injecting power into the grid after switching ON the switch on the DC side. About $40\,s$ later it reached the steady-state operation.

Figure 12 Smart microgrid installed in Castrelos' Aquaculture Centre

After that, it continued to extract power, oscillating around the MPP due to the voltage perturbation introduced by the MPPT algorithm of the inverter.

Before switching ON the input breaker of the PV inverter, the DC open-circuit voltage (V_{DCoc}) was approximately $186\,V$ and $252\,V$ with generators 80-7s-2p and PGS 100R, respectively. This means that an over-voltage protection circuit is not needed since the maximum input DC voltage of the PV inverter is $400\,V$.

Figure 6 shows the overlap of the safe operating areas of Solax X1-0.7 PV inverter and 80-7s-2p generator that are installed on-site. The V_{DC} operating voltage is about 55 V, just above the lower limit of the MPPT range (V_{MPPmin}). For the nominal water flow ($25\,l/s$), this voltage would increase. In any case, the (no-load) output voltage constant of the generator should not be lower than $0.199\,V/rpm$.

From Figure 6, the compatibility is ensured since the start operating voltage is $V_{DCstart} = 70\,V_{DC}$, and the MPPT voltage range is 50-380 V_{DC}. In addition, the maximum input voltage, $V_{DCmax} = 400\,V$, is sufficiently higher than V_{DCoc} that the over-voltage protection circuit is not required.

6. Conclusions

This paper described the design of an effective grid connection approach for a pico-hydro system based on an overshot waterwheel. It is based on the integration of a permanent magnet synchronous generator and a photovoltaic (PV) inverter. Three generators and a conventional PV inverter were used for evaluation purposes. Following this approach, the waterwheel was connected to a microgrid and it is operating in an

aquaculture centre, taking advantage of the waterfall in one of its tanks, with a head of $2\ m$ and a flow rate of only about $13\ l/s$. This pico-hydro system injects $126\ W$ into the grid, with a global efficiency of about 50%.

This work demonstrates how hydroelectric energy can be generated on a very small-scale, properly integrated into existing infrastructures and, therefore, without the need for any civil construction works. On the other hand, it demonstrates how the generated energy can be injected into the grid, in a simple and effective way, using only equipment widely available on the market.

For the connection to the utility grid, the generator's three-phase voltage system is converted to a DC voltage. Then, a conventional PV inverter (through its MPPT algorithm) controls the operating point of the waterwheel, i.e., the rotational speed and torque, by controlling, respectively, the voltage (V_{DC}) and current (I_{DC}) at the output of the rectifier bridge.

This work also demonstrates that an additional over-voltage protection circuit can be dispensed by suitably selecting the gearbox ratio and generator's constants W/rpm and V/rpm.

The compatibility between a pico-hydro turbine and the PV inverter was analysed in detail. The use of a PV inverter offers an effective (robust, flexible, efficient, economical, and "plug and play") interface with the utility grid. It is believed that these results will be of the utmost importance for many companies installing distributed generation systems. On the other hand, they may contribute to the widespread exploitation of small hydro resources untapped so far and without environmental impact. However, it should be emphasised that not all PV inverters may be compatible with hydro generation. The dynamics of the MPPT algorithm and especially the way it is initiated may make the use of some inverters unfeasible.

7. Declaration of competing interest

8. Acknowledgements

9. Funding

10. Authors contributions

Vicente Leite was responsible for the project management, idea conception, implementation, data collection, methodology, formal analysis, and manuscript's writing.

11. Data availability statement

The data in the paper were obtained on site, by recording videos with the values given by multimeters measuring the DC voltage and current. The AC power was obtained from the PV inverter itself. The data in Figure 8, for generators AFPMG260, PGS 100R and 80-7s-2p were acquired, respectively, on 21 December 2020, 23 February 2021 and 9 June 2021. The data in Figures 9, 10 and 11 were acquired on 9 June 2021.
The author confirms that the data supporting the results of this study are fully presented in the appendix.

12. Appendix

This section provides the data used to obtain Figures 8 to 11. Appendix I shows the data used to obtain the $P - V$ curves of the waterwheel with the 3 generators. Appendix II presents the data used to obtain the $P_{DC} - V_{DC}$ and $I_{DC} - V_{DC}$ characteristics for different water flows. The AC power data, at the PV inverter output, during the starts with generators 80-7s-2p and PGS 100 are presented in Appendix III.

Appendix I:
Data used to obtain the P-V curves of the waterwheel with 3 different generators.

AFPMG260			PGS 100R			80-7s-2p		
V_{DC} (V)	I_{DC} (A)	P_{DC} (W)	V_{DC} (V)	I_{DC} (A)	P_{DC} (W)	V_{DC} (V)	I_{DC} (A)	P_{DC} (W)
78.4	1.7	136.9	138.8	0.9	119.9	151.5	0.3	45.5
70.2	2.1	145.5	134.8	0.9	121.8	146.2	0.4	53.5
61.9	2.4	149.3	130.1	1.0	124.1	141.3	0.4	60.7
58.4	2.6	154.3	126.7	1.0	123.7	136.2	0.5	67.3
51.8	3.0	153.6	122.4	1.0	124.9	131.2	0.6	75.3
50.8	3.0	153.8	117.9	1.1	126.2	125.3	0.7	81.9
50.1	3.1	155.1	112.5	1.1	127.8	121.0	0.7	87.1
49.9	3.1	154.3	106.8	1.2	128.8	115.7	0.8	92.1
49.0	3.2	154.5	100.6	1.3	129.5	110.7	0.9	97.0
47.8	3.2	152.1	93.7	1.4	127.4	105.6	1.0	103.1
46.3	3.3	150.6	86.0	1.5	126.9	100.4	1.1	106.4
45.4	3.3	151.6	81.1	1.6	127.0	95.3	1.2	111.3
34.1	4.1	140.5	77.0	1.6	124.7	90.2	1.3	115.6
			74.2	1.7	123.7	85.1	1.4	118.1
			73.0	1.7	123.9	80.8	1.5	121.7
			69.0	1.8	120.8	75.0	1.7	125.0
			65.0	1.8	118.2	71.1	1.8	126.2
			61.5	1.9	116.7	65.4	2.0	128.7
			56.2	2.0	113.0	59.6	2.2	129.7
			51.2	2.1	108.8	54.6	2.4	129.9
			46.9	2.2	103.6	50.4	2.6	129.4
						45.2	2.8	128.6
						40.5	3.1	127.0
						35.4	3.5	123.6
						30.6	3.9	119.7

Appendix II:
Data used to obtain the P_{DC}-V_{DC} and I_{DC}-V_{DC} characteristics for different water flows.

Higher water flow			Intermediate water flow			Lower water flow		
V_{DC} (V)	I_{DC} (A)	P_{DC} (W)	V_{DC} (V)	I_{DC} (A)	P_{DC} (W)	V_{DC} (V)	I_{DC} (A)	P_{DC} (W)
151.5	0.3	45.5	146.1	0.3	42.4	120.6	0.2	29.0
146.2	0.4	53.5	140.0	0.4	51.0	114.9	0.3	33.3
141.3	0.4	60.7	136.0	0.4	55.8	110.2	0.3	38.3
136.2	0.5	67.3	131.9	0.5	62.2	104.9	0.4	42.4
131.2	0.6	75.3	125.0	0.5	68.5	100.2	0.5	46.9
125.3	0.7	81.9	120.0	0.6	73.2	95.3	0.5	50.7
121.0	0.7	87.1	115.1	0.7	79.0	90.4	0.6	53.1
115.7	0.8	92.1	110.6	0.7	82.7	85.4	0.7	56.8
110.7	0.9	97.0	105.2	0.8	88.0	80.0	0.8	60.0
105.6	1.0	103.1	100.3	0.9	91.4	75.0	0.8	62.5
100.4	1.1	106.4	95.0	1.0	96.3	69.2	0.9	65.0
95.3	1.2	111.3	89.8	1.1	98.8	64.7	1.0	67.4
90.2	1.3	115.6	84.8	1.2	102.7	60.3	1.1	69.2
85.1	1.4	118.1	80.5	1.3	104.3	56.0	1.3	71.7
80.8	1.5	121.7	75.1	1.4	106.4	50.0	1.4	72.2
75.0	1.7	125.0	69.9	1.6	109.0	45.0	1.6	72.7
71.1	1.8	126.2	65.7	1.7	111.3	41.1	1.8	74.1
65.4	2.0	128.7	60.2	1.9	113.1	35.6	2.1	73.1
59.6	2.2	129.7	54.5	2.1	112.4	30.6	2.3	70.1
54.6	2.4	129.9	50.5	2.3	113.9	25.0	2.7	68.2
50.4	2.6	129.4	45.3	2.5	112.7	20.5	3.1	63.7
45.2	2.8	128.6	40.5	2.8	111.4	15.8	3.6	57.3
40.5	3.1	127.0	35.2	3.1	109.4	11.0	4.2	46.5
35.4	3.5	123.6	29.6	3.5	104.9			
30.6	3.9	119.7	24.9	3.9	98.5			

Appendix III:
Data regarding the AC power, at the PV inverter output, during the starts with generators 80-7s-2p and PGS 100.

Start up with the 80-7s-2p generator

t(s)	P_{AC} (W)	t(s)	P_{AC} (W)	t(s)	P_{AC} (W)
102.0	0.0	154.0	126.0	204.0	126.0
104.0	6.0	155.0	117.0	205.0	131.0
105.0	12.0	156.0	124.0	206.0	127.0
106.0	15.0	157.0	124.0	207.0	123.0
107.0	38.0	158.0	128.0	208.0	120.0
108.0	91.0	159.0	125.0	209.0	122.0
109.0	79.0	160.0	127.0	210.0	126.0
110.0	108.0	161.0	122.0	211.0	125.0
111.0	121.0	162.0	125.0	212.0	129.0
112.0	92.0	163.0	127.0	213.0	128.0
113.0	105.0	164.0	137.0	214.0	122.0
114.0	106.0	165.0	129.0	215.0	124.0
115.0	110.0	166.0	126.0	216.0	126.0
116.0	99.0	167.0	121.0	217.0	123.0
117.0	121.0	168.0	126.0	218.0	128.0
118.0	118.0	169.0	128.0	219.0	127.0
119.0	117.0	170.0	127.0	220.0	130.0
120.0	116.0	171.0	123.0	221.0	131.0
121.0	112.0	172.0	126.0	222.0	123.0
122.0	108.0	173.0	121.0	223.0	122.0
123.0	112.0	174.0	124.0	224.0	126.0
124.0	115.0	175.0	117.0	225.0	125.0
125.0	115.0	176.0	126.0	226.0	128.0
126.0	112.0	177.0	127.0	227.0	122.0
127.0	113.0	178.0	131.0	228.0	129.0
128.0	117.0	179.0	127.0	229.0	122.0
129.0	116.0	180.0	123.0	230.0	129.0
130.0	124.0	181.0	131.0	231.0	127.0
131.0	120.0	182.0	130.0	232.0	127.0
132.0	120.0	183.0	124.0	233.0	123.0
133.0	121.0	184.0	122.0	234.0	129.0
134.0	123.0	185.0	129.0	235.0	128.0
135.0	122.0	186.0	131.0	236.0	129.0
136.0	120.0	187.0	126.0	237.0	122.0
137.0	116.0	188.0	132.0	238.0	121.0
138.0	125.0	189.0	125.0	239.0	125.0
139.0	130.0	190.0	124.0	240.0	127.0
140.0	127.0	191.0	127.0	241.0	122.0
141.0	113.0	192.0	121.0	242.0	129.0
142.0	123.0	193.0	128.0	243.0	119.0
143.0	120.0	194.0	127.0	244.0	127.0
144.0	118.0	195.0	126.0	245.0	122.0
145.0	126.0	196.0	129.0	246.0	128.0
146.0	126.0	197.0	120.0	247.0	124.0
147.0	128.0	198.0	126.0		
148.0	114.0	199.0	121.0		
150.0	124.0	200.0	123.0		
151.0	126.0	201.0	127.0		
152.0	130.0	202.0	125.0		
153.0	125.0	203.0	129.0		

Start up with the PGS 100 generator

t(s)	P_{AC} (W)	t(s)	P_{AC} (W)	t(s)	P_{AC} (W)
102.0	0.0	149.0	109.0	196.0	125.0
103.0	8.0	150.0	117.0	197.0	117.0
104.0	4.0	151.0	123.0	198.0	118.0
105.0	11.0	152.0	123.0	199.0	118.0
106.0	33.0	153.0	117.0	200.0	118.0
107.0	39.0	154.0	120.0	201.0	127.0
108.0	102.0	155.0	126.0	202.0	125.0
109.0	96.0	156.0	118.0	203.0	129.0
110.0	113.0	157.0	124.0	204.0	120.0
111.0	102.0	158.0	120.0	205.0	120.0
112.0	91.0	159.0	126.0	206.0	122.0
113.0	105.0	160.0	123.0	207.0	121.0
114.0	96.0	161.0	119.0	208.0	119.0
115.0	106.0	162.0	114.0	209.0	122.0
116.0	109.0	163.0	120.0	210.0	116.0
117.0	109.0	164.0	124.0	211.0	119.0
118.0	98.0	165.0	121.0	212.0	116.0
119.0	100.0	166.0	114.0	213.0	118.0
120.0	111.0	167.0	117.0	214.0	116.0
121.0	109.0	168.0	124.0	215.0	123.0
122.0	108.0	169.0	124.0	216.0	121.0
123.0	109.0	170.0	119.0	217.0	121.0
124.0	113.0	171.0	124.0	218.0	119.0
125.0	98.0	172.0	121.0	219.0	119.0
126.0	109.0	173.0	123.0	220.0	121.0
127.0	122.0	174.0	117.0	221.0	122.0
128.0	108.0	175.0	125.0	222.0	118.0
129.0	105.0	176.0	118.0	223.0	122.0
130.0	111.0	177.0	125.0	224.0	114.0
131.0	116.0	178.0	125.0	225.0	118.0
132.0	107.0	179.0	117.0	226.0	109.0
133.0	112.0	180.0	117.0	227.0	115.0
134.0	112.0	181.0	124.0	228.0	113.0
135.0	119.0	182.0	127.0	229.0	115.0
136.0	117.0	183.0	125.0	230.0	112.0
137.0	116.0	184.0	123.0	231.0	113.0
138.0	114.0	185.0	114.0	232.0	117.0
139.0	116.0	186.0	125.0	233.0	124.0
140.0	114.0	187.0	130.0	234.0	118.0
141.0	120.0	188.0	122.0	235.0	115.0
142.0	118.0	189.0	122.0	236.0	117.0
143.0	120.0	190.0	119.0	237.0	117.0
144.0	116.0	191.0	118.0	238.0	112.0
145.0	117.0	192.0	122.0	239.0	123.0
146.0	114.0	193.0	121.0	240.0	122.0
147.0	114.0	194.0	120.0		
148.0	123.0	195.0	121.0		

References

[1] I. E. Agency. (2021) Net zero by 2050: A roadmap for the global energy sectors. [Online]. Available: https://iea.blob.core.windows.net/assets/deebef5d-0c34-4539-9d0c-10b13d840027/NetZeroby2050-ARoadmapfortheGlobalEnergySector_CORR.pdf

[2] U. Nations. (2019) World small hydropower development report 2019. [Online]. Available: https://www.unido.org/sites/default/files/files/2020-08/Global_overview.pdf

[3] I. H. Association. (2021) Hydropower status report sector - trends and insights. [Online]. Available: https://assets-global.website-files.com/5f749e4b9399c80b5e421384/60c37321987070812596e26a_IHA20212405-status-report-02_LR.pdf

[4] M. Pérez-Sánchez, F. Sánchez-Romero, H. Ramos, and P. López-Jiménez, "Energy recovery in existing water networks: Towards greater sustainability," *MDPI Special Issue Water Systems towards New Future Challenges*, vol. 9, no. 2, 2017. [Online]. Available: https://doi.org/10.3390/w9020097

[5] S. Morales, L. Corredor, J. Paba, and L. Pacheco, "Stages in the development of a small hydropower project: Context and implementation basic criteria," *Dyna*, vol. 81, no. 184, pp. 178–185, 2014. [Online]. Available: https://doi.org/10.15446/dyna.v81n184.39757

[6] A. Kadier, M. S. Kalil, M. Pudukudy, H. A. Hasan, A. Mohamed, and A. A.Hamid, "Pico hydropower (php) development in malaysia: Potential, present status, barriers and future perspectives," *Renewable and Sustainable Energy Reviews*, vol. 81, no. 2, pp. 2796–2805, Jan. 2018. [Online]. Available: https://doi.org/10.1016/j.rser.2017.06.084

[7] T. S. Kishore, E. R. Patro, V. S. Harish, and A. T. Haghighi, "A comprehensive study on the recent progress and trends in development of small hydropower projects," *Energies*, vol. 14, May 2021. [Online]. Available: https://doi.org/10.3390/en14102882

[8] M. Molina and M. Pacas, "Improved power conditioning system of microhydro power plant for distributed generation applications," in *International Conference on Industrial Technology (ICIT)*, 2010, pp. 1733–1738. [Online]. Available: https://doi.org/10.1109/ICIT.2010.5472461

[9] K. R. Sharma, S. Kewat, and B. Singh, "Energy recovery robust 3IMPL control algorithm for power management of SyRG/PV/BES-Based distributed islanded microgrid," *IEEE Transactions on Industrial Electronics*, vol. 66, no. 10, Oct. 2019. [Online]. Available: https://doi.org/10.1109/TIE.2018.2880673

[10] P. Kerdtuad, T. Simma, K. Chaiamarit, and S. Visawaphatradhanadhorn, "Establishment of a pico hydro power plant using permanent magnet synchronous generator supplied for AC microgrid," in *44th Annual Conference of the IEEE Industrial Electronics Society (IECON)*, 2018. [Online]. Available: https://doi.org/10.1109/IEECON.2018.8712214

[11] P. Peña-Carro, O. Izquierdo-Monge, L. Hernández-Callejo, and G. Martín-Jiménez, "Small wind turbines study and integration in a peri-urban microgrid," *Revista Facultad de Ingeniería Universidad de Antioquia*, no. 104, pp. 108–117, Jul-Sep 2022. [Online]. Available: https://doi.org/10.17533/udea.redin.20210845

[12] M. Ospina-Quiroga and E. Mojica-Nava, "Distributed optimal control for distribution systems with microgrids," *Revista Facultad de Ingeniería Universidad de Antioquia*, no. 105, pp. 98–110, Oct-Dec 2022. [Online]. Available: https://doi.org/10.17533/udea.redin.20211164

[13] P. Shapes, "Work package 5: Energy recovery in existing infrastructures with small hydropower plants, multipurpose schemes - overview and examples."

[14] E. C. Arrieta, S. A. Flórez, and N. I. Sierra, "Application of CFD to the design of the runner of a propeller turbine for small hydroelectric power plants," *Revista Facultad de Ingeniería Universidad de Antioquia*, no. 69, pp. 181–192, 2013. [Online]. Available: http://www.scielo.org.co/scielo.php?script=sci_arttext&pid=S0120-62302013000400015

[15] K. Sopian and J. Razak, "Pico hydro: Clean power from small streams," in *3rd WSEAS Int. Conf. on Renewable Energy Sources*, 2009, pp. 414–419. [Online]. Available: https://asset-pdf.scinapse.io/prod/2606848680/2606848680.pdf

[16] J. Titus and B. Ayalur, "Design and fabrication of in-line turbine for pico hydro energy recovery in treated sewage water distribution line," *Elsevier, Energy Procedia*, vol. 156, pp. 133–138, 2019. [Online]. Available: https://doi.org/10.1016/j.egypro.2018.11.117

[17] D. Satish, A. Doshi, and M. Bade, "Review on pump as turbine application in water distribution networks for power generation," in *AIP Conference Proceedings 2341, 030035*, 2021. [Online]. Available: https://doi.org/10.1063/5.0050115

[18] V. Leite, "Overshot waterwheel based grid-connected pico-hydro system," in *IV Ibero-American Conference on Smart Cities*, Mexico, 2021.

[19] N. Koirala, R. Dhakal, D. Lubitz, D. Bhandari, G. Dev, Y. Dhakal, and U. Niraula, "Review of low head turbines system of nepal for rural electrification," in *6th International Conference on Renewable Energy Research and Applications (ICRERA)*, 2017, pp. 861–869. [Online]. Available: https://doi.org/10.1109/ICRERA.2017.8191182

[20] V. P. Chandran, S. Murshid, and B. Singh, "Voltage and frequency controller with power quality improvement for PMSG based pico-hydro system," in *IETE Journal of Researcha*, Chennai, India, 2018. [Online]. Available: https://doi.org/10.1109/PEDES.2018.8707810

[21] B. Pali and S. Vadhera, "An innovative continuous power generation system comprising of wind energy along with pumped-hydro storage and open well," *IEEE Transactions on Sustainable Energy*, vol. 11, no. 1, pp. 145–153, 2020. [Online]. Available: https://doi.org/10.1109/TSTE.2018.2886705

[22] K. R. Vasudevan, V. K. Ramachandaramurthy, V. Gomathi, J. B. Ekanayake, and S. K. Tiong, "Modelling and simulation of variable speed pico hydel energy storage system for microgrid applications," *Elsevier Journal of Energy Storage*, vol. 24, pp. 1–14, 2019. [Online]. Available: https://doi.org/10.1016/j.est.2019.100808

[23] N. F. Yah, A. N. Oumer, and M. S. Idris, "Small scale hydro-power as a source of renewable energy in malaysia: A review," *Elsevier Renewable and Sustainable Energy Reviews*, vol. 72, pp. 228–239, 2017. [Online]. Available: https://doi.org/10.1016/j.rser.2017.01.068

[24] D. K. Okot, "Review of small hydropower technology," *Elsevier Renewable and Sustainable Energy Reviews*, vol. 26, pp. 515–529, 2013. [Online]. Available: https://doi.org/10.1016/j.rser.2013.05.006

[25] V. Leite, J. Couto, A. Ferreira, and J. Batista, "A practical approach for grid-connected pico-hydro systems using conventional photovoltaic inverters," in *International Energy Conference (ENERGYCON)*, Leuven, Belgium, 2016, pp. 1–6. [Online]. Available: https://doi.org/10.1109/ENERGYCON.2016.7513911

[26] G. Ribeiro, W. Silva, V. Leite, and A. Ferreira, "Grid connection approach for very small-scale pico-hydro systems using pv microinverters," in *45th Annual Conference of the IEEE Industrial Electronics Society (IECON)*, Lisbon, Portugal, 2019. [Online]. Available: https://doi.org/10.1109/IECON.2019.8926691

[27] M. Rahimi, "Modeling, control and stability analysis of grid-connected pmsg based wind turbine assisted with diode rectifier and boost converter," *Elsevier International Journal of Electrical Power & Energy Systems*, vol. 93, pp. 84–96, 2017. [Online]. Available: https://doi.org/10.1016/j.ijepes.2017.05.019

[28] I. Scotta, W. Silva, and V. Leite, "Overvoltage protection for grid-connected pico-hydro generation using photovoltaic inverters," *Revista Facultad de Ingeniería, Universidad de Antioquia*, vol. 99, pp. 73–82, 2021. [Online]. Available: https://doi.org/10.17533/udea.redin.20200581

[29] G. Müller and K. Kauppert, "Performance characteristics of water wheels," *Journal of Hydraulic Research*, vol. 42, no. 5, pp. 451–460, 2004. [Online]. Available: https://doi.org/10.1080/00221686.2004.9641215

[30] E. Quaranta and R. Revelli, "Hydraulic behavior and performance of breastshot water wheels for different numbers of blades," *Journal of Hydraulic Engineering*, vol. 143, no. 1, 2017. [Online]. Available: https://doi.org/10.1061/(ASCE)HY.1943-7900.0001229

[31] L. Figueiredo, W. Silva, and V. Leite, "Implementation of a smart microgrid in a small museum: the silk house," *Springer Communications in Computer and Information Science book series*, vol. 1152, 2020. [Online]. Available: https://doi.org/10.1007/978-3-030-38889-8_10

[32] E. Quaranta, "Investigation and optimization of the performance of gravity water wheels," Ph.D. Thesis, Politecnico di Torino, 2017. [Online]. Available: https://core.ac.uk/download/pdf/84252843.pdf

[33] E. Quaranta and R. Revelli, "Performance characteristics, power losses and mechanical power estimation for a breastshot waterwheel," *Elsevier Energy*, vol. 87, no. 1, pp. 315–325, 2015. [Online]. Available: https://doi.org/10.1016/j.energy.2015.04.079

[34] Overshot water wheel design calculator. Borst Engineering & Construction LLC. Accessed Jan. 3, 2022. [Online]. Available: https://www.borstengineeringconstruction.com/Overshot_Water_Wheel_Design_Calculator.html

[35] V. Polidorio, "Design and analysis of an overshot water wheel for a grid-connected pico-hydro system," MSc Thesis, Polytechnic Institute of Bragança, 2020. [Online]. Available: http://hdl.handle.net/10198/23880

[36] J. Laghari, H. Mokhlis, A. Bakar, and H. Mohammad, "A comprehensive overview of new designs in the hydraulic, electrical equipments and controllers of mini hydropower plants making it cost effective technology," *Elsevier Renewable and Sustainable Energy Reviews*, vol. 20, p. 279–293, 2013. [Online]. Available: https://doi.org/10.1016/j.rser.2012.12.002

[37] D. Gonzalez, C. A. R. Parra, A. J. S. Montes, E. I. A. Zuluaga, and C. E. Carrejo, "Modeling and control of grid connected photovoltaic systems," *Revista Facultad de Ingeniería Universidad de Antioquia*, no. 62, pp. 145–156, 2012. [Online]. Available: http://www.scielo.org.co/pdf/rfiua/n62/n62a15.pdf

[38] T. F. Guimarães and V. Leite, "Analyses of mppt algorithms in real test conditions," in *9th International Conference on Renewable Energy Research and Application (ICRERA)*, Glasgow, UK, 2020. [Online]. Available: https://doi.org/10.1109/ICRERA49962.2020.9242873

[39] S. Kouro, J. I. Leon, D. Vinnikov, and L. G. Franquelo, "Grid-connected photovoltaic systems: An overview of recent research and emerging PV converter technology," *IEEE Industrial Electronics Magazine*, vol. 9, no. 1, pp. 47–61, 2015. [Online]. Available: https://doi.org/10.1109/MIE.2014.2376976

[40] N. Mohan, T. M. Undeland, and W. P. Robbins, *Power Electronics: Converters, Applications, and Design*, 3rd ed. Tonawanda, NY: John Wiley & Sons, Inc, 2003.

[41] A. Urtasun, P. Sanchis, I. Martín, J. López, and L. Marroyo, "Modeling of small wind turbines based on PMSG with diode bridge for sensorless maximum power tracking," *Elsevier Renewable Energy*, vol. 55, pp. 138–149, 2013. [Online]. Available: https://doi.org/10.1016/j.renene.2012.12.035

[42] D. W. Hart, *Power Electronics*. NY 10020.: McGraw-Hill, 2011.

[43] V. Caliskan, D. Perreault, T. Jahns, and J. Kassakiano, "Analysis of three-phase rectifiers with constant-voltage loads," *IEEE Transactions on Circuits and Systems I: Fundamental Theory and Applications*, vol. 50, no. 9, pp. 1220–1225, 2003. [Online]. Available: https://doi.org/10.1109/TCSI.2003.816323

[44] (2016) Smart drive applications for diy projects - applications manual. EcoInnovation. Accessed Jan. 3, 2022. [Online]. Available: https://drive.google.com/file/d/0BzVDBix3S_qbNnZvbDByQUhIcjA/view?resourcekey=0-_MFlLhtc_rqvP55ZBEDtoA

[45] C. P. Ion and C. Marinescu, "Hydro turbine emulator for micro hydro power plants," *AGIR Bulletin*, vol. 4, pp. 143–148, 2012. [Online]. Available: https://www.agir.ro/buletine/1528.pdf

[46] A. Ansel and B. Robyns, "Modelling and simulation of an autonomous variable speed micro hydropower station," *Elsevier Mathematics and Computers in Simulation*, vol. 71, no. 4-6, pp. 320–332, 2006. [Online]. Available: https://doi.org//10.1016/j.matcom.2006.02.011

[47] Planning guidelines - flexible storage system with battery-backup function. SMA. Accessed: September, 2020. [Online]. Available: https://files.sma.de/downloads/SI44M-80H-13-BBF-IA-en-10.pdf

[48] Sunny island 3.0m/4.4m/6.0h/8.0h and sunny remote control – operating manual. SMA. Accessed: September, 2020. [Online]. Available: https://www.europe-solarstore.com/download/sma/sunnyisland/SI30M-44M-60H-80H-BE-en-30W.pdf

[49] Sunny home manager 2.0 – operating manual. SMA. Accessed: September, 2020. [Online]. Available: https://files.sma.de/downloads/HM-20-BE-en-18.pdf